lubricants

MDPI

Article

Modeling Inertia-Driven Oil Transport Inside the Three-Piece Oil Control Ring of Internal Combustion Engines

Tsung-Yu Yang, Mo Li and Tian Tian *

Department of Mechanical Engineering, Massachusetts Institute of Technology, 77 Massachusetts Ave., Cambridge, MA 02139, USA; tyyang@mit.edu (T.-Y.Y.); moli@mit.edu (M.L.)
* Correspondence: tiantian@mit.edu

Abstract: The three-piece oil control ring (TPOCR), traditionally used in light-duty gasoline engines, is becoming a viable option for heavy-duty gas and hydrogen engines due to its ability to control lubricating oil consumption (LOC) under throttled conditions. Understanding the distribution of oil inside the TPOCR groove, as well as the effects of rail gap and drain hole positions, is critical for optimizing TPOCR and groove designs. In this work, a one-dimensional oil distribution model was developed to simulate inertia-driven oil transport in the TPOCR groove. A novel approach was proposed by first dividing the TPOCR into units composed of a pair of expander pitches. Then, the relationship between the oil outflow rate of the unit and its oil mass was established with the help of three-dimensional two-phase computational fluid dynamics (CFD) simulations. This relationship was then used to model one-dimensional oil transport along the circumference of the TPOCR groove. Incorporating the boundary conditions at the rail gaps and drain holes, this simple model can complete computations for 10,000 cycles within a few seconds, allowing for quick the evaluation of transient behavior and design iterations. Studies on low-load conditions show that the model, with reasonable adjustment for the boundary conditions, can match the oil distribution patterns observed in visualization experiments. This is the first step toward studying oil transport in the TPOCR groove before involving the effects of gas flows.

Keywords: engine lubrication; lubricating oil consumption (LOC); three-piece oil control ring (TPOCR); computational fluid dynamics (CFD); numerical model

Citation: Yang, T.-Y.; Li, M.; Tian, T. Modeling Inertia-Driven Oil Transport Inside the Three-Piece Oil Control Ring of Internal Combustion Engines. *Lubricants* **2024**, *12*, 394. https://doi.org/10.3390/lubricants12110394

Received: 11 October 2024
Revised: 6 November 2024
Accepted: 11 November 2024
Published: 16 November 2024

1. Introduction

In internal combustion engines, oil control rings play a crucial role in controlling the oil supply and significantly impacting lubricating oil consumption. TPOCRs have been widely adopted in modern engines due to their efficient oil control and reduced oil consumption. Although the use of TPOCRs has become prevalent, research on this topic remains notably lacking.

The oil control ring shown in Figure 1 consists of three components, the upper rail, expander, and lower rail. Each ring has a gap for ease of installation, and these gaps serve as critical paths for oil transport. The upper and lower rails create a barrier to regulate the oil flow, while the expander functions as a spring, providing tension force to the rails to seal the ring/liner interface. The function of the top ring is to control high pressure gas entering the ring pack. The oil control rings regulate the oil supply to the top two rings and control the oil film thickness on the liner [1–4]. The second ring acts as a buffer, providing secondary control for both oil and gas. In addition to controlling the upward oil flow, the oil control ring is a favorable path for the release of the oil after performing the lubrication function in the upper regions. The release function of the oil control ring is largely accomplished through the drain holes inside the oil control ring groove [5–7].

Figure 1. Sample piston (**left**) and three-piece oil control ring (**right**).

A critical parameter for both oil leakage into the ring pack and its release is the oil accumulation inside the oil control ring groove, as it determines the oil boundary conditions along the leakage and release paths. There are three main oil leakage paths in the oil control ring: (1) the upper rail gap, (2) the ring/liner interface, and (3) the groove itself. The extent of oil leakage from these regions is directly influenced by the amount of oil accumulated in the groove.

The upper rail gap is the most direct path for oil to reach the upper region. Under zero blowby conditions, significant oil leakage can occur through this gap, as noted in [8,9]. When oil accumulation reaches a certain level, oil bridging may occur, causing oil to adhere to the liner and leak through the ring/liner interface. Additionally, oil can also leak through the upper flank between the upper rail and the oil control ring groove.

The primary source of oil to the oil control ring is through the lower rail gap. While drain holes are intended to release oil from the groove, under certain conditions, they can also act as a source of oil. Another source of oil to the oil control ring groove is the upper flank between the upper rail and the oil control ring groove. Oil can accumulate above the upper rail during up-scraping, and this oil may transfer to the piston.

These processes, illustrated in Figure 2, demonstrate that the amount of oil leakage is heavily dependent on the oil accumulation inside the groove. Therefore, developing a model to estimate the oil accumulation in the groove is crucial. However, the understanding of oil accumulation in the oil control ring groove is still very limited. Previous studies on TPOCR oil transport and its effect on LOC showed that the level of LOC increases during the transition from low to high load conditions [10,11]. Operating under the blow-by separation line (low load) conditions leads to high LOC, with oil accumulation in the TPOCR groove tending to be higher at low loads and low engine speeds [9].

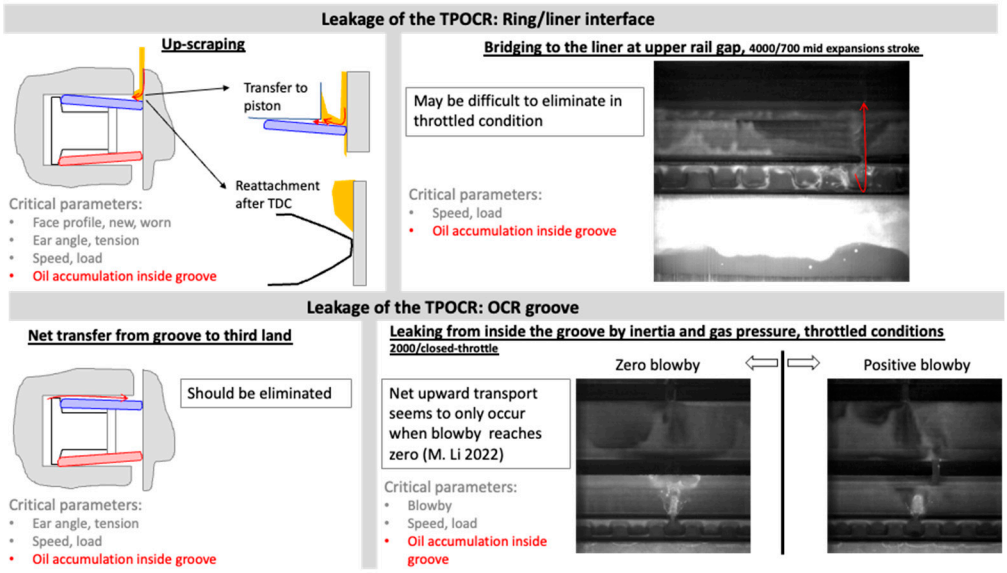

Figure 2. Oil leakage mechanism [9].

To better understand and predict these phenomena, numerous physical models have been devised with the aim of predicting gas flow and oil transport in the piston ring pack [12–17]. Tian [14] developed a TPOCR model by coupling the ring dynamics and lubrication to study friction, asperity contact, and oil transport between rails/grooves, rails/liners, and rails/expanders. The model assumes that the third land pressure is constant, and the region between the rails and groove is filled with oil. To accurately predict oil transport through the rail/groove clearance, Zhang [15] employed two-phase mass-conserved fluid sub-models for the oil/gas flow through the rail/groove clearance. While the oil transport in the contact regions in these models can be accurately described by the Reynolds equation, a more sophisticated method is required for non-contact regions, such as the oil flow below the lower rail, through the gaps, and inside the groove. Fang [16] conducted a study on oil transport using CFD followed by the development of simplified models and correlations to predict oil flow rates in two non-contact regions: (1) below the oil control ring in the space between the skirt chamfer and the liner; and (2) the space between the piston ring pack and the liner. This study provides an appropriate oil dynamic pressure boundary condition at the outer entrance of the clearance between the lower rail and its groove. To accurately model oil transport across TPOCR, Riken Corporate [17] developed models for the TPOCR motion in the groove and the oil transport behavior using the Computer Aided Engineering (CAE) method. The model consists of two parts: (1) the TPOCR motion model; and (2) the oil transport model. The TPOCR motion model calculates the three-dimensional ring motion and torsional deformation using Finite Element Analysis (FEA). The oil transport model is a two-phase flow CFD model that utilizes the ring motion from TPOCR motion, taking an arbitrary two-dimensional cross-section to calculate oil leakage to the third land. These models have been verified by experimental results and show good agreement. It is important to note that all these models are two-dimensional models that only consider oil transport in the radial and axial directions on piston lands and/or oil control ring grooves. However, oil distribution along the circumferential direction in the groove is critical for accurately estimating oil leakages through the TPOCR and determining the optimal arrangement of the drain holes, which are highly related to oil consumption.

This work aims to develop a fast oil distribution model for predicting oil distribution along the circumferential direction within the oil control ring groove. Initially, CFD analysis was applied to study oil transport in the TPOCR groove and establish a correlation between oil accumulation and the flow rate. This correlation was then used in the development of a one-dimensional model to predict the oil distribution along the groove. The model's accuracy was validated through comparison with CFD results for short-term simulations, and further validated against experimental results to assess its long-term performance.

The paper is organized as follows. Section 2 describes the experimental setup and observations. Section 3 details the CFD simulation settings. Section 4 outlines the proposed oil redistribution model and presents the results. Section 5 provides a parametric study of the model, analyzing the effects of various factors, and the conclusion is presented in Section 6.

2. Two-Dimensional LIF Experiment

2.1. Setup

For the observation of oil transport in the ring pack, the 2D Laser Induced Fluorescence technique (2D-LIF) was applied to an optical single-cylinder prototype engine. The engine originated from a four-cylinder port injection PSA product engine with 3 cylinders deactivated on the cylinder head. A custom-made engine liner with a sapphire window on the thrust side was applied to observe oil transport. The choice of sapphire was made as it has a similar thermal expansion coefficient as steel, the material that made up the rest of the liner, in order to provide good sealing and comfortability when fired up. Located at the middle of the thrust side, the window was 12 mm wide and 98.5 mm long and counted for 16 degrees of the whole circumferential direction given the 86.6 mm bore. Figure 3 shows the optical liner and the overall test engine setup. A detailed description of the engine running parameter can be found in Table 1.

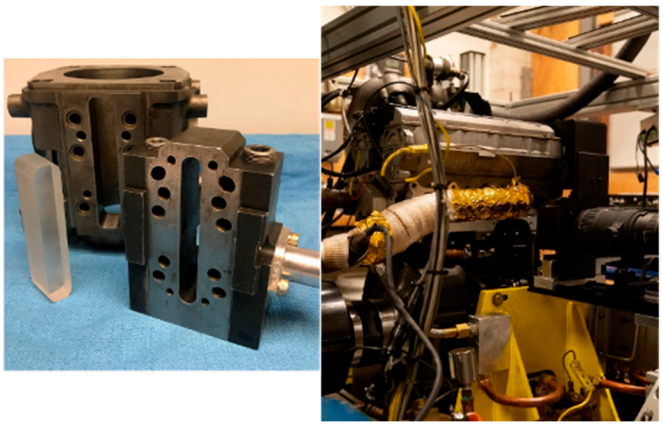

Figure 3. Optical liner and test engine setup.

Table 1. Engine specifications.

Engine Characters	
Type	Spark Ignition 4 Valves
Bore	86.6 mm
Stroke	88.0 mm
Displacement	0.511 L
Max specific power	37.3 kW/L@5400 RPM
Max specific torque	80 Nm/L@4200 RPM
Lubricant	SAE 0W20

A specific dye was mixed with the lubricant oil which can be induced to fluorescence using a laser. The oil was stored in an external reservoir and was fed into and extracted out from the engine through two recirculating pumps. In addition, due to the sensitivity of the fluorescence signal to temperature, a temperature control device was applied in the oil circulation loop to feed the oil into the engine at 50 °C ± 1 °C. An Photron SA-X2 high-speed camera was used to capture the video through the optical window and allowed for the observation of oil transport in the ring pack and skirt region. The maximum resolution of the camera is 1024 × 1024 pixels focused on a 12 mm ×12 mm square area. The highest frame rate that can be achieved without sacrificing resolution is 12,500 fps, converting to around one frame per crank angle at 2000 RPM. Figure 4 shows an optical image from the high-speed camera, where the brighter part means a thicker oil film thickness and the darker part indicates less oil. A detailed description of the 2D-LIF engine setup and optical theory can be found in [18].

Specifically, two camera operations were defined, namely high-speed control and low-speed control. The high-speed camera control can record the path of the piston moving up and down starting from the intake TDC. The slow-speed camera control records one frame per engine cycle at a chosen CA position. This can make the piston appear stationary in the video and can be used for analyzing the oil flow pattern's change over longer time scales. The laser, high-speed camera, and engine operation were controlled and synchronized through the FPGA system.

The piston and ring pack was chosen as a barrel-shaped top ring with a positive twist, a second ring with a Napier hook chamfer design on the outer diameter (OD), and a modern low-tension TPOCR. The top ring gap was pinned in the center of the optical window for better observation.

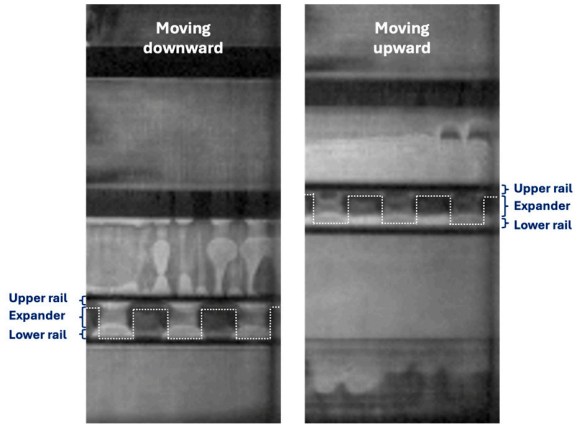

Figure 4. Oil transport during BDC.

2.2. Observation

Figures 4 and 5 illustrate the behavior of oil transport during the transition between the piston's downward and upward movements, and vice versa. As the piston reaches the bottom dead center (BDC), driven by the downward inertial force, the oil in the pitch with higher thickness hits the lower rail, forming a puddle. When the piston starts its upward motion, with the downward inertial force, the oil in the expander spreads out to neighboring units and forms a flattened film, as illustrated in Figure 4. Conversely, at the top dead center (TDC), the oil similarly hits the upper rail, forming a puddle, and upon the downward motion, the oil redistributes between the adjacent pitches and forms a flattened film, as depicted in Figure 5. An additional note is that the oil bridging from the piston to the liner occurs when the piston moves toward the BDC and the TDC. In the areas with bridged oil, the trailing rail becomes fully flooded and, thus, increases the oil leakage through the rail/liner interface locally. The higher the oil accumulation inside the TPOCR groove is, the earlier the bridging occurs with a longer duration. Increasing the upper rail leakage from the liner, caused by higher oil accumulation through oil bridging, is one of the main reasons to increase the understanding of the oil accumulation inside the TPOCR groove. There are two driving forces for the redistribution and accumulation pattern inside the oil ring groove, namely inertia and bridging. The observations shown in Figures 4 and 5 are the combined results of the two forces mentioned above. Figure 6 is an illustration showing the effects separately. Currently, there is no numerical study of this distribution process within the groove. Therefore, developing a numerical study and a predictive model for oil distribution in the oil control ring groove is essential for advancing our understanding and improving the overall design. This work is focused on the inertia effect, which is always present, in contrast to the gas flow effect, which is only effective locally and during certain periods of a cycle.

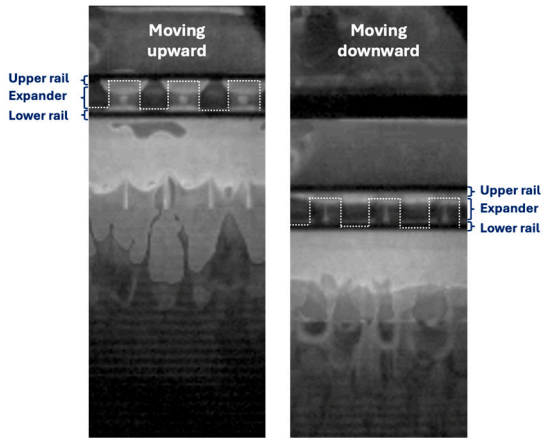

Figure 5. Oil transport during TDC.

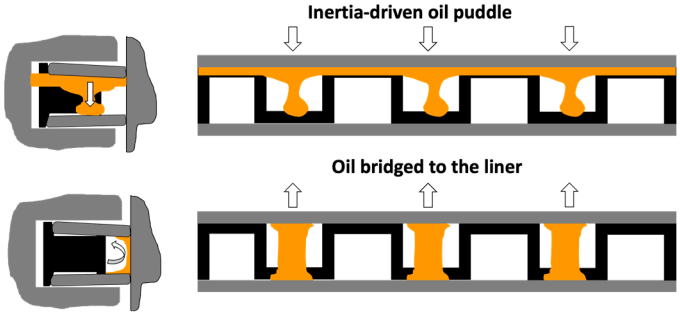

Figure 6. An illustration of an inertial force-driven oil puddle and oil bridging to the liner.

3. CFD Simulation

To investigate the oil transport mechanisms within the oil control ring groove, three-dimensional simulations were conducted using Ansys Fluent (Version 2024R2), a commercial CFD software widely used in industrial applications. The simulations employed the Volume of Fluid (VOF) model to capture the interface between the oil and gas phases [19]. Figure 7 illustrates the three-dimensional computational domain, which includes the lower gap and the oil control ring groove.

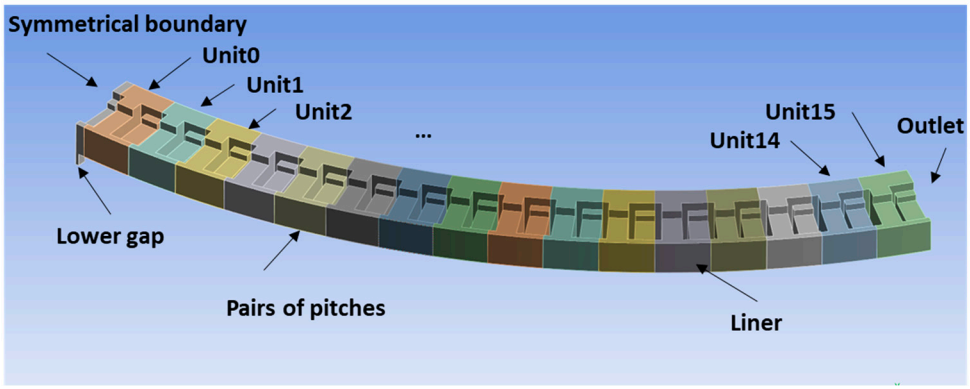

Figure 7. The computational domain of the TPOCR model.

In these CFD simulations, the clearance between the oil control ring rail/land and the liner was ignored due to its negligible size compared to other dimensions, as it was not the primary focus of this study. To optimize computational efficiency, the model was simplified to include only a segment consisting of 16 pairs of pitches. This reduction was considered sufficient for analyzing the slow oil transport process along the groove.

The mesh for the CFD simulations, depicted in Figure 8, was generated using Ansys Meshing. A polyhedral mesh was chosen for its superior accuracy in representing complex geometries, offering better resolution of geometric features, and conforming well to the simulated object. The mesh size was set to 100 µm around the gap and 200 µm away from the gap.

This study focuses on inertia-driven flow, deliberately excluding the effects of gas flow. Consequently, no pressure difference was considered within the groove. The computational domain was defined by the following boundary conditions:

1. Pressure Inlet/Outlet: This was applied to the lower gap during down/up strokes, with the pressure set at 1 bar.
2. Pressure Inlet/Outlet: This was applied to the outlet during up/down strokes, with the pressure set at 1 bar.
3. Symmetry: This was applied to the surface adjacent to the lower gap.
4. Moving surface: This was applied to the liner, with the velocity determined based on engine speed.

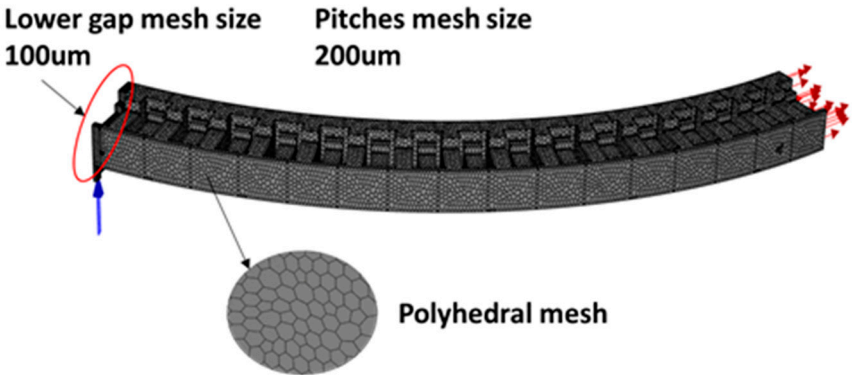

Figure 8. CFD mesh for TPOCR model.

In the simulation, the lubricant was introduced through the lower gap during down strokes and expelled during up strokes. The inlet volume fraction was set to 0.1, representing a 10 μm oil film on the liner below the TPOCR. The piston was used as the reference frame; therefore, the piston liner velocity was defined as the inverse of the piston's instantaneous velocity. A contact angle of 45° was assigned to all solid wall surfaces. The simulation started from the top dead center position and spanned 20 engine revolutions, ensuring comprehensive oil distribution to regions beyond the gap.

3.1. Oil Distribution Model

While there used to be many different types of expanders, the ES-80 type expander has gradually become the most popular type. As shown in Figure 1 and referenced in the SAE piston ring-grooves standard [20], the expander exhibits an alternating pattern along its circumference. A pitch with the horizontal bar on the top is followed by one on the bottom. Due to the space occupied by the horizontal bar, oil accumulation between the two adjacent pitches differs. Consequently, when the inertia shifts direction, the pitch with a higher accumulation experiences earlier oil movement. This movement, driven by inertia, varies between pitches. For this reason, we divided the expander into units with each unit composed of two pitches, as illustrated in Figure 9. During the transition from upstrokes to downstrokes, oil in the left pitch with an expander exceeds that in the right pitch without an expander. As the inertial force shifts upward, oil from the lower rail begins to move to the upper rail. Once the oil puddle reaches the upper rail, it disperses laterally from the left pitch to the right pitch, eventually reaching equilibrium. At equilibrium, the right pitch holds more oil than the left pitch. Conversely, when the inertial force shifts downward, the oil flows from right pitch back to the left pitch. By considering these upward and downward forces together, the oil flows both upstream and downstream, as illustrated in Figure 10. The outflow rate from each unit is a function of the oil volume it contains, the engine speed, the oil density, and the oil viscosity. This relationship can be expressed as follows:

$$Q(V,\ E,\ \mu) = \frac{a\rho V^b E^c d_{flank}}{\mu^d}$$

where Q represents the oil outflow rate from a unit, ρ denotes the oil density, V denotes the oil volume in a unit, E stands for the engine speed, d_{flank} denotes the depth of the flank, and μ denotes the oil viscosity. The parameters a, b, c, and d, are obtained by fitting the CFD results. The outflow rate Q depends on the oil volume, engine speed, oil density, and viscosity, characterizing the flow to both upstream and downstream units. This form was chosen to capture the effects of key parameters on the oil flow rate: the oil volume, density engine speed, and ring groove size positively correlated with the flow rate, while oil viscosity, which resists flow, has a negative correlation.

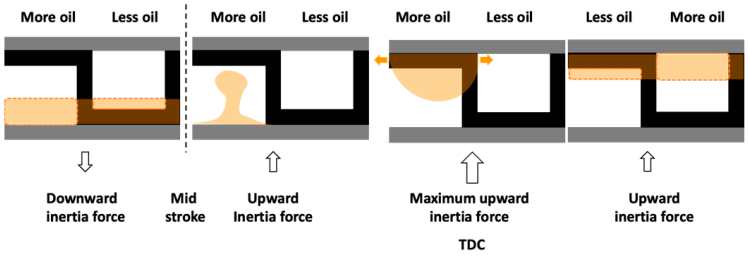

Figure 9. Oil transport mechanism within a unit.

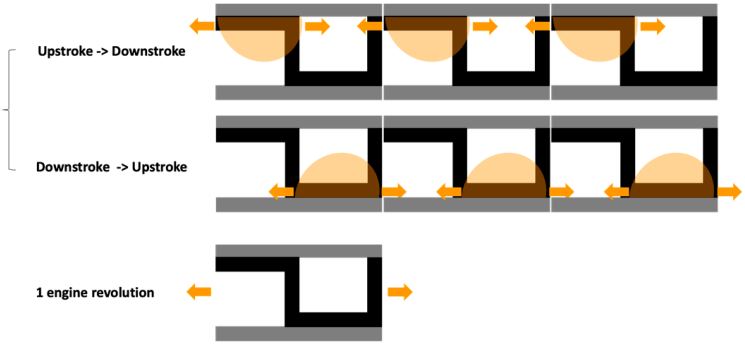

Figure 10. Oil transport mechanism between units.

The net flow rate for $unit_i$ is derived as follows:

- The upstream net flow rate between $unit_i$ and $unit_{i-1}$

$$Q\left(V_{i-1}^n,\ E, \mu\ \right) - Q(V_i^n, E, \mu)$$

- The downstream net flow rate between $unit_i$ and $unit_{i+1}$

$$Q\left(V_{i+1}^n, E, \mu\right) - Q(V_i^n, E, \mu)$$

Therefore, the total net flow for $unit_i$ is the combination of the upstream and downstream net flows:

$$Net\ flow\ for\ unit_i = Q\left(V_{i-1}^n, E, \mu\right) - 2Q(V_i^n, E, \mu) + \left(V_{i+1}^n, E, \mu\right)$$

The oil distribution model, describing the change in oil volume within a unit, can be formulated as follows:

$$V_i^{n+1} = V_i^n + \Delta t\left(Q\left(V_{i-1}^n, E, \mu\right) - 2Q(V_i^n, E, \mu) + Q\left(V_{i+1}^n, E, \mu\right)\right) + \Delta t\left(Q_{i==lower\ gap}\right)$$

where V_i^{n+1} represents the oil volume in $unit_i$ at time step $n + 1$, and Δt is the time for 1 engine revolution. The lower gap acts as the primary oil source for this model, with the amount of oil assumed to be constant. The drain holes serve as outlet boundary conditions, allowing oil to exit the groove. By fixing the oil volume at a specific value at the drain holes, the modeling results closely align with the experimental observations.

3.2. Fitting CFD Results

The oil flow rate through the boundary and the oil mass in each unit were calculated from CFD simulations. The simulation result at crank angle 3590° is shown in Figure 11. The yellow regions represent the oil volume fractions.

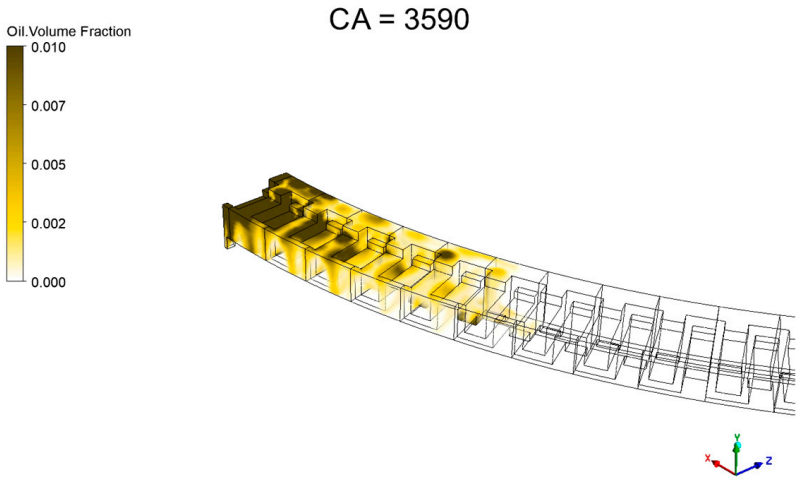

Figure 11. CFD simulations after 3590° crank angles.

To determine the average effect of oil transport within one engine revolution, the oil flow rate and oil volume were averaged over each revolution. However, after performing the averaging, the flow rate across the boundary between units represented the net flow. To correlate the outflow and oil volume, further data processing was required.

To extract the outflow through the boundary from the net flow, the first empty unit ($unit_{i+1}$) in the groove must be identified. Since there was no outflow from $unit_{i+1}$ to $unit_i$, the outflow of $unit_i$ to $unit_{i+1}$ could be calculated by the oil volume change in $unit_{i+1}$. The outflow of $unit_{i-1}$ could then be obtained by subtracting the net flow of $unit_i$ from the outflow of $unit_i$. This procedure was applied iteratively to obtain the outflow for all other units. An illustration of this process is shown in Figure 12. By compiling all the data, the coefficients a, b, c, and d in Equation 1 could be obtained.

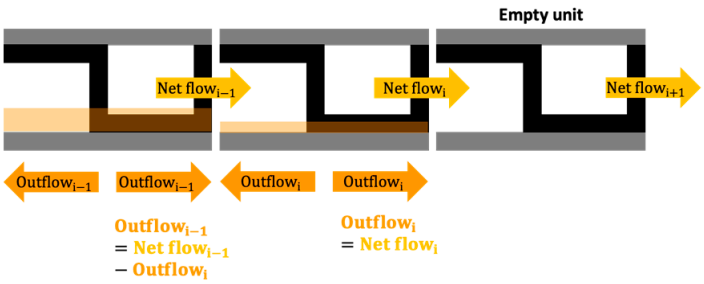

Figure 12. Concept of oil distribution model.

4. Result

4.1. CFD Result

The oil volume and outflow rate at an engine speed of 1000 RPM are shown in Figures 13 and 14. It can be seen that, except for $unit_0$, the oil transports slowly along the groove, with the oil only reaching $unit_8$ after eight cycles. $unit_0$ displays a clear periodic pattern due to its proximity to the lower gap, where oil can flow in and out quickly. The oil flow rate through the boundary fluctuates without a clear pattern, making it unreliable for establishing a correlation for oil transport within the groove. Therefore, $unit_0$ and $unit_1$ were excluded from the analysis when building the correlation for oil transport.

Figures 15 and 16 present the oil volume and outflow rate after data processing, showing clearer trends. It can be clearly seen that both the oil volume and oil outflow rate gradually increase, although the rate of growth slows over time. Figure 17 shows the correlation between the oil accumulation and mass flow rate through the boundary. Each line depicts the change in oil accumulation and mass flow rate for each unit over time. The dots represent the amount of oil and flow rates for each revolution. The dots near the lower

left correspond to the initial stages of oil accumulation, while those toward the upper right reflect data after more engine revolutions. The proposed equation effectively reflects the behavior observed in the CFD results. The derived regression equation is as follows:

$$Q(V, E) = 0.002 \frac{\rho V^{1.40} E^{1.86} d_{flank}}{\mu^{0.38}}$$

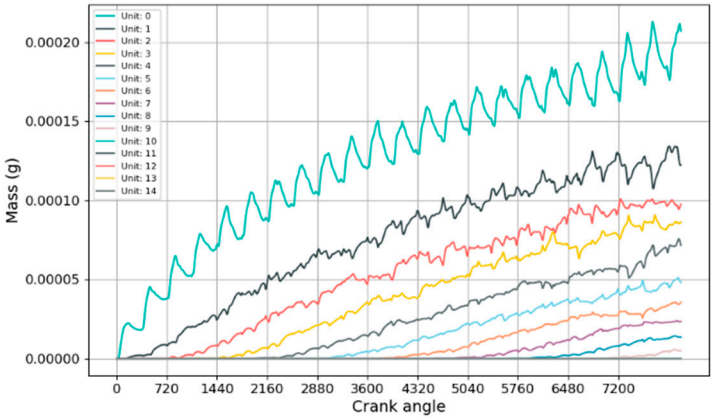

Figure 13. Oil accumulation in the groove (E: 1000 RPM, μ: 0.0036 $\frac{\text{kg}}{\text{m·s}}$).

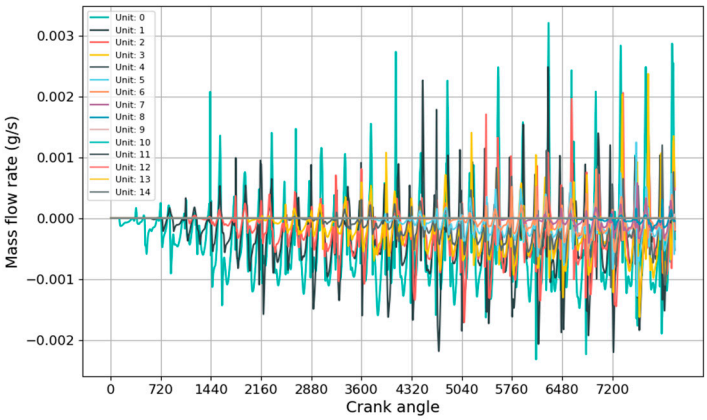

Figure 14. Oil mass flow rate (E: 1000 RPM, μ: 0.0036 $\frac{\text{kg}}{\text{m·s}}$).

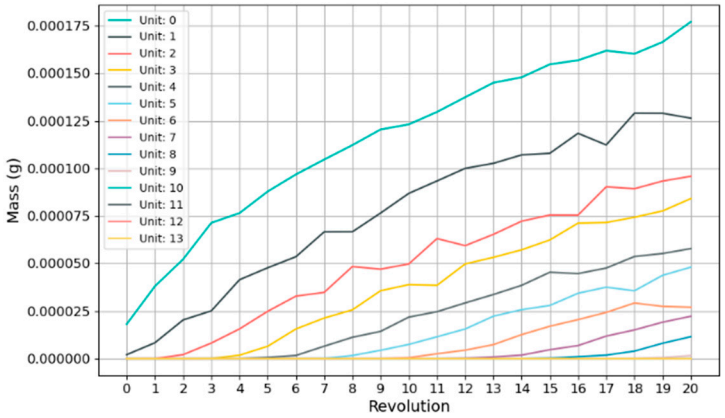

Figure 15. Oil accumulation after data processing (E: 1000 RPM, μ: 0.0036 $\frac{\text{kg}}{\text{m·s}}$).

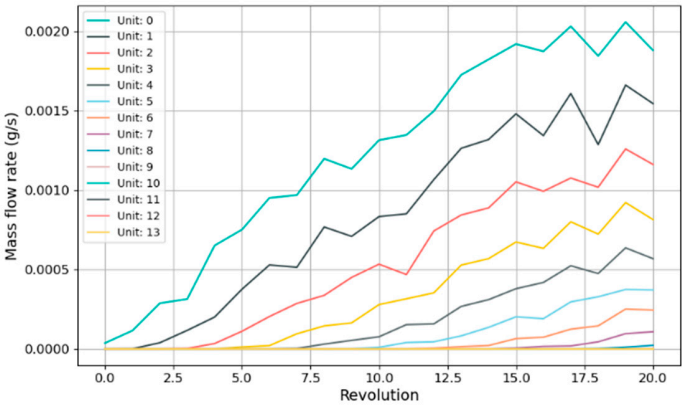

Figure 16. Oil mass flow rate after data processing (E: 1000 RPM, μ: 0.0036 $\frac{\text{kg}}{\text{m}\cdot\text{s}}$).

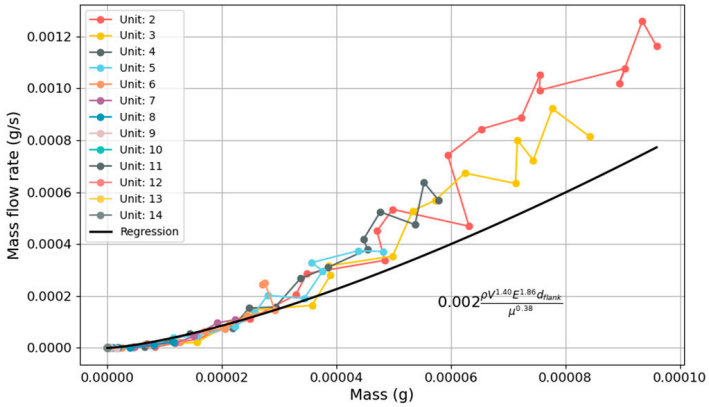

Figure 17. Correlation between oil accumulation and mass flow rate (E: 1000 RPM, μ: 0.0036 $\frac{\text{kg}}{\text{m}\cdot\text{s}}$).

The equation reveals that the correlation between the oil accumulation and flow rate is nonlinear and exhibits a trend stronger than linear. This means that the oil outflow rate increases more rapidly than the oil volume. In cases of low oil volume, there is not enough oil to move from one pitch to its neighbors. Additionally, when only a thin oil film is present, significant capillary forces can further restrict oil transport.

The relationship between engine the speed and flow rate is also nonlinear and has a more pronounced impact than oil volume. The correlation for different engine speeds is shown in Figure 18. Oil transport is more stable at lower engine speeds, as indicated by the dots aligning well with the regression results. In contrast, at higher engine speeds, the dots spread more widely, indicating greater instability. Nevertheless, the proposed method can still effectively capture these trends.

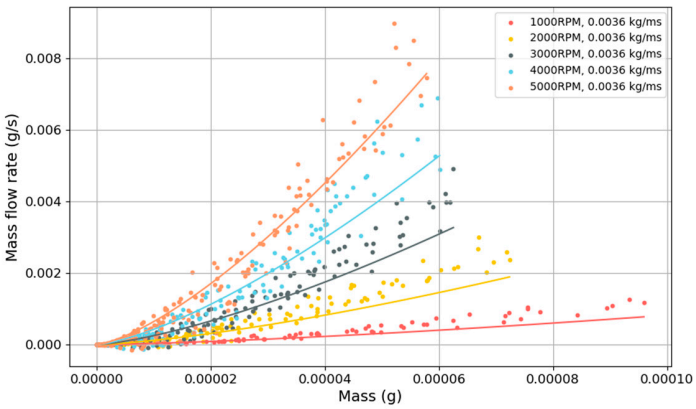

Figure 18. Correlation between oil accumulation and mass flow rate (μ: 0.0036 $\frac{\text{kg}}{\text{m}\cdot\text{s}}$).

4.2. Comparison of CFD and Oil Distribution Model

To validate the oil distribution model and ensure accuracy in predicting oil distribution within the groove, the model was compared against CFD results through simulations replicating CFD settings. A model comprising 14 units was constructed for this purpose, excluding units 0 and 1 as they are adjacent to the lower gap and do not represent typical oil transport behavior in the groove. The boundary conditions of this simplified model used the mass flow rate of unit 1 derived from CFD results. The simulations covered 20 revolutions to be compared with the CFD results.

Figures 19 and 20 illustrate the comparison of the modeling results with CFD outcomes at engine speeds of 1000 RPM and 5000 RPM, respectively. The findings demonstrate that the oil distribution model closely aligns with the CFD results, indicating that oil accumulation increases rapidly initially and slows after several engine revolutions. This behavior can be explained by the oil distribution model, where the oil volume in a unit is determined by the outflow from the unit and the inflow from its neighboring unit. Units with less oil receive more from their neighbors, gradually reducing the differences in oil volume until equilibrium is reached, at which point there is no oil exchange between the units.

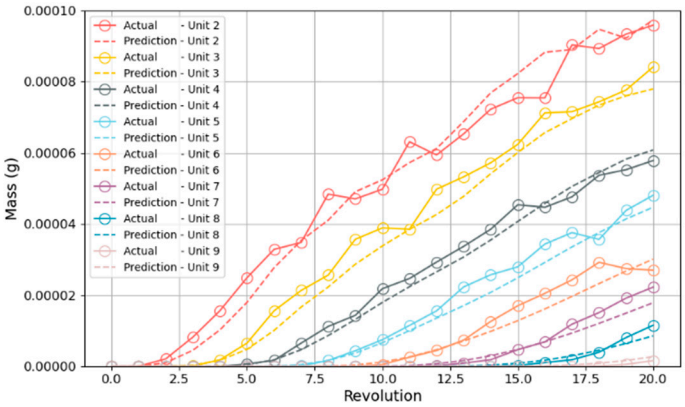

Figure 19. Comparison of oil distribution model and CFD simulations (E: 1000 RPM, μ: 0.0036 $\frac{\text{kg}}{\text{m·s}}$).

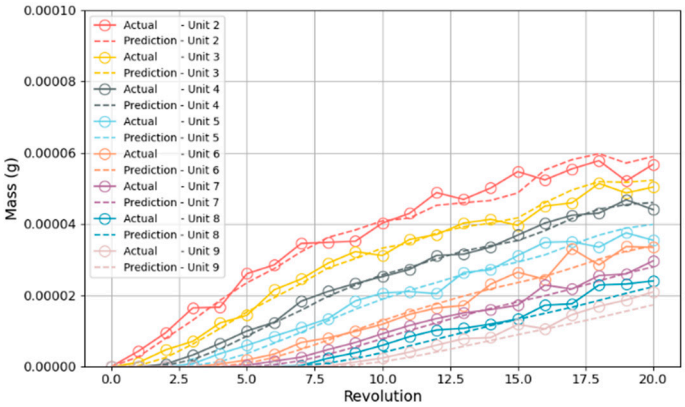

Figure 20. Comparison of oil distribution model and CFD simulations (E: 5000 RPM, μ: 0.0036 $\frac{\text{kg}}{\text{m·s}}$).

Figure 21 shows the comparison of CFD results and the prediction from the oil distribution model across various engine speeds and viscosities, with an R^2 value of 0.97, indicating a high degree of correlation. Additionally, the oil distribution model takes just a few seconds to complete the calculation, making it significantly more efficient than CFD simulations.

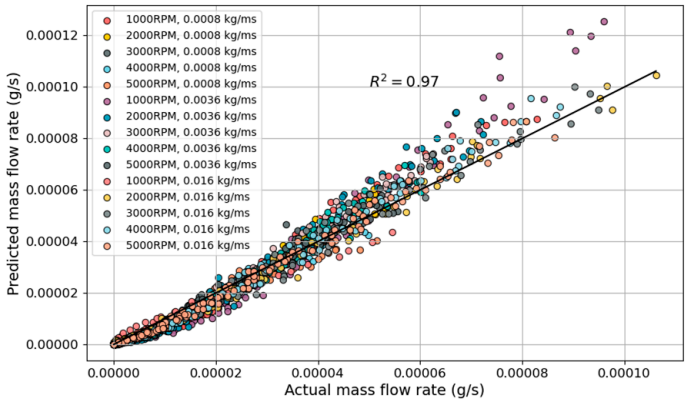

Figure 21. Predicted values from oil distribution model vs. actual values from CFD.

4.3. Comparison of Oil Distribution Model and Experiment Results

The primary objective of this model is to predict oil distribution over several thousand engine revolutions, a task unfeasible with CFD due to computational limitations. Consequently, CFD cannot be used to verify the oil distribution model developed here for long-term predictions; instead, experimental results must be used for validation. To compare with experimental results, a model replicating the experimental setup was developed. The oil control ring used in the experiment comprised 101 units with four drain holes on the piston. Observations during the experiments indicated that the oil control ring could rotate along the circumferential direction, and in this study, the rotation speed was approximately 2000 revolutions for the ring to complete one full rotation [9]. This rotational effect, which significantly impacts oil distribution in the groove, was incorporated into the model. The oil density was 800 $\frac{\text{kg}}{\text{m}^3}$ and the viscosity was 0.016 $\frac{\text{kg}}{\text{m}\cdot\text{s}}$. The oil inflow through the lower gap was assumed to be a 20 µm oil film on the skirt, representing a typical thickness for demonstration purposes in the model. Oil entered the groove through the lower gap primarily when it was within the skirt regions, and only a 1 µm oil film was considered on the liner when the lower gap was outside these regions. Parametric studies were conducted and are provided in the next section to explore the dependency of the oil accumulation on the thickness of the oil film passing by the piston skirt.

Figures 22–24 illustrate the oil distribution in the oil control ring groove at different stages. The *x*-axis represents the piston's position, while the *y*-axis indicates oil accumulation in the groove, quantified as the ratio of empty space filled with oil.

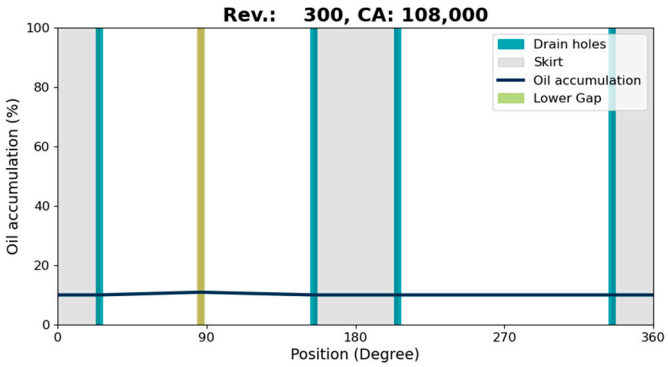

Figure 22. Oil accumulation in the oil control ring groove after 300 engine revolutions.

Figure 22 shows oil distribution in the groove after 300 engine revolutions, where the lower gap is outside the skirt region, resulting in minimal oil entering the groove. Figure 23 displays the modeling results after 800 revolutions, where the lower gap aligns with the skirt region, providing a more substantial oil source from the lower gap and, thus, greater oil accumulation in the groove. Once the lower gap passes the skirt region, the oil

accumulation in the groove decreases as the oil disperses and drains out through the drain holes, as illustrated in Figure 24.

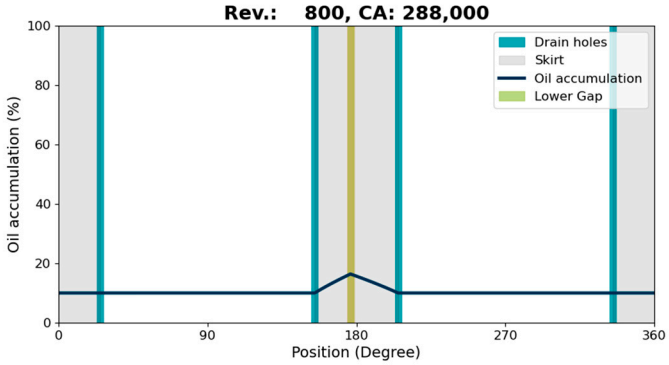

Figure 23. Oil accumulation in the oil control ring groove after 800 engine revolutions.

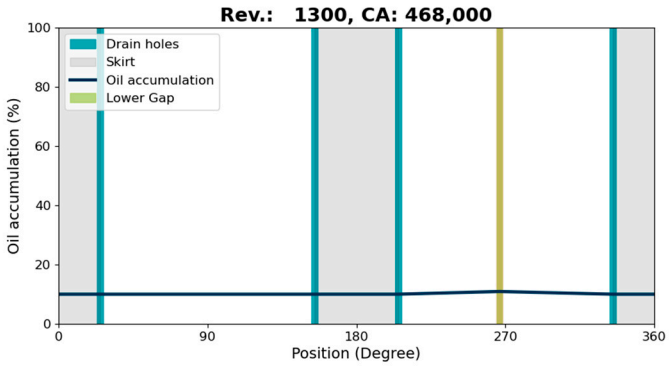

Figure 24. Oil accumulation in the oil control ring groove after 1300 engine revolutions.

In the experiments, the oil distribution could only be observed through the observation window. For comparison between experimental and modeling results, the oil accumulation at the center of the skirt was analyzed. Figure 25 provides an illustration and an example photo, showing the location of each component of the TPOCR. In the figure, the brighter regions represent lubricating oil, while the black areas indicate empty space. The picture was taken at a 76° CA intake stroke where the inertial force changed direction. Thus, it represents an accumulated effect of the upward inertial force that pushed the oil leveled inside the groove to the upper flank. Since the 2D-LIF technique only allows for observation at a shallow depth behind the window, with the oil level flat, it can be used to represent the oil accumulation in the whole volume. Based on that, a computer vision tool was applied to detect the brightness in the videos and quantify the oil accumulation level. Detailed information about this method has been discussed in previous studies [9]. Although there is no linear relationship between oil accumulation and brightness, this method serves as the best estimation to quantitatively compare the oil accumulation inside the groove.

Since the exact amount of oil cannot be measured directly, computer vision techniques were employed to quantify the oil volume. Brightness was used as a proxy for the amount of oil in the oil control ring groove.

Figure 26 shows a result from the experiment conducted at 2000 RPM under low load conditions, where the effect of gas flow is minimal. As the oil control ring rotates, the oil source from the lower gap also rotates. The region adjacent to the lower gap tends to accumulate more oil, resulting in less oil in the remaining regions. Experimentally, it was observed that when the lower gap is within the observation window, local oil accumulation increases, as reflected by a rise in intensity increase, with about 80% to 90% of the oil control ring groove filled with oil. Once the lower gap moves past the observation window, the oil accumulation level recovers as well as the measured brightness intensity,

and approximately 50% of the oil control ring groove is filled with oil. Based on these observations, the boundary condition at the drain hole is assumed to be the same oil occupation observed in the experiment when the lower rail gap is away.

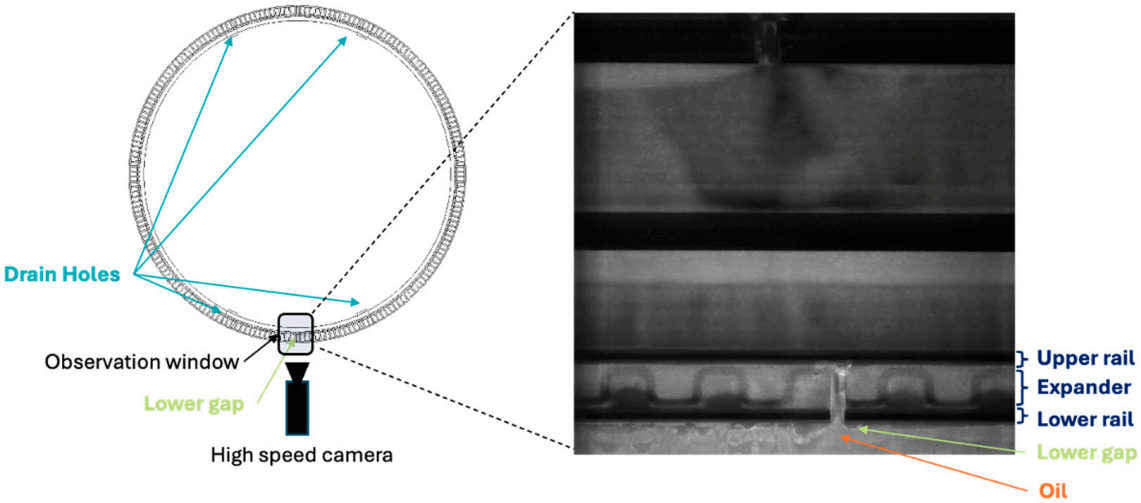

Figure 25. Illustration of observation region (**left**) and example of observation photo from experiment (**right**).

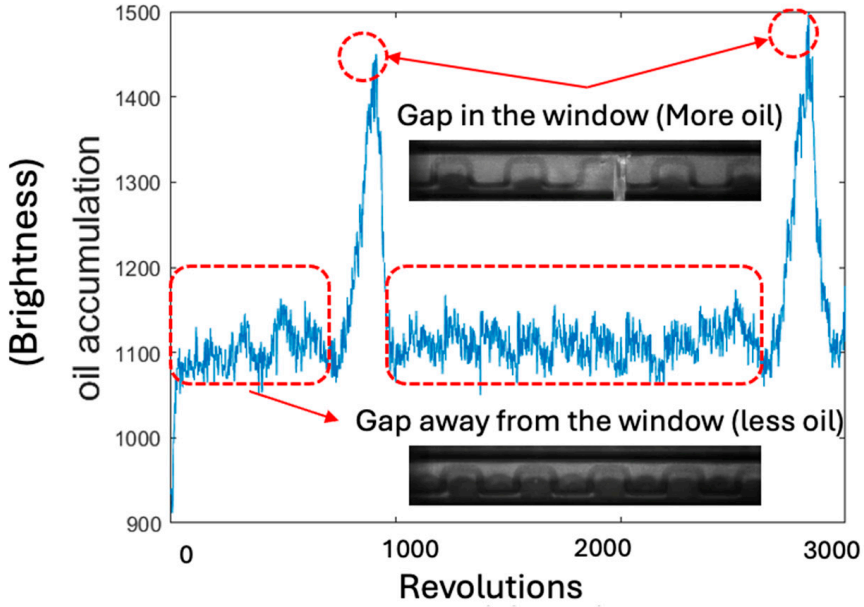

Figure 26. Experimental observation of oil accumulation.

To compare experimental and modeling results, Figure 27 presents the modeling result of oil accumulation at the center (180 degrees). The observed pattern closely matches the experimental findings, demonstrating that the model accurately represents oil distribution in the groove with adequate boundary conditions. Although the boundary condition was adjusted to align with the experimental setup, this insight can guide the development of accurate boundary conditions for the drain hole in future studies.

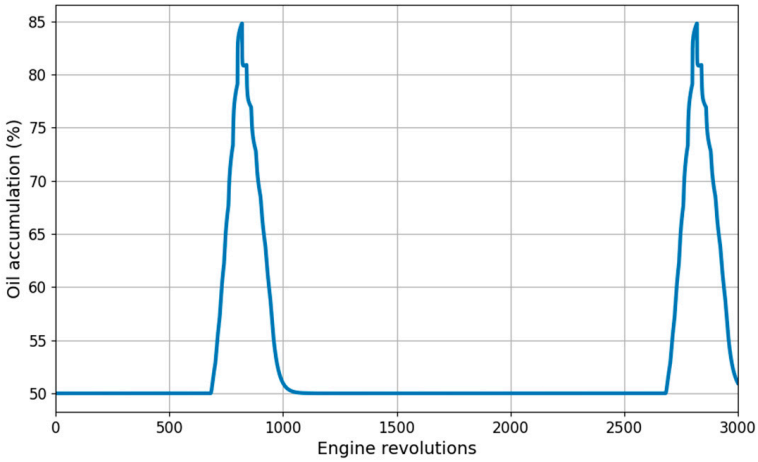

Figure 27. Modeling result of oil accumulation.

5. Parametric Study

The oil distribution model was applied to simulate various scenarios, including the oil film thickness, the engine speed, the oil viscosity, and the number and arrangement of drain holes. The maximum oil accumulation in the groove was used as the metric for analyzing oil accumulation, as it directly influences the extent of oil leakage through the oil control ring.

5.1. Comparison of Different Oil Film Thickness

The oil film thickness determines the amount of oil flowing into the groove through the lower rail gap during the engine's downstroke. The oil inflow rate can be estimated using the following equation:

$$Q_{oil} = \frac{h \cdot w_{gap} \cdot L_{stroke} \cdot E}{60}$$

where Q_{oil} is the oil inflow rate, h is the oil film thickness, w_{gap} is the gap width (0.377 mm), L_{stroke} is the stroke length (88 mm), and E represents engine speed (2000 RPM). This study considers four drain holes, with the arrangement as shown in Figure 22. The results reveal that a thicker oil film on the liner allows more oil to flow into the groove, leading to greater oil accumulation. The highest oil accumulation occurred between revolutions 750 to 1000, 1750 to 2000, and 2750 to 3000, corresponding to when the lower gap enters the skirt region. Figure 28 presents these results.

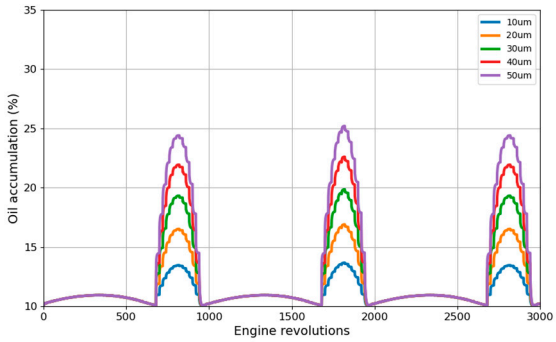

Figure 28. Effect of oil film thickness on oil accumulation.

5.2. Comparison of Different Engine Speeds

Figure 29 illustrates the effect of engine speed on oil accumulation, with the oil film thickness set at 20 µm. The results demonstrate that as the engine speed increases, less oil accumulates in the groove.

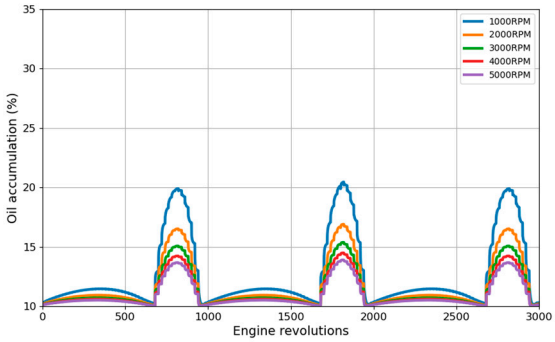

Figure 29. Effect of engine speed on oil accumulation.

5.3. Comparison of Different Number of Drain Holes

There is currently limited research on the arrangement of drain holes. This section examines the impact of varying numbers and configurations of drain holes. To explore the effect of the number of drain holes on oil accumulation, scenarios with 1, 2, 4, and 6 drain holes were compared. In all cases, the drain holes were placed on the pin side, which is the most common configuration. Figure 30 shows the placement of the drain holes. The modeling results, depicted in Figure 31, indicate that the number of drain holes significantly affects oil accumulation. As the number of drain holes increases, oil accumulation in the groove decreases. This occurs because, under low load conditions, inertial forces are the primary mechanism driving oil out of the groove. With more drain holes, additional exit paths are provided for the oil, thereby reducing oil accumulation.

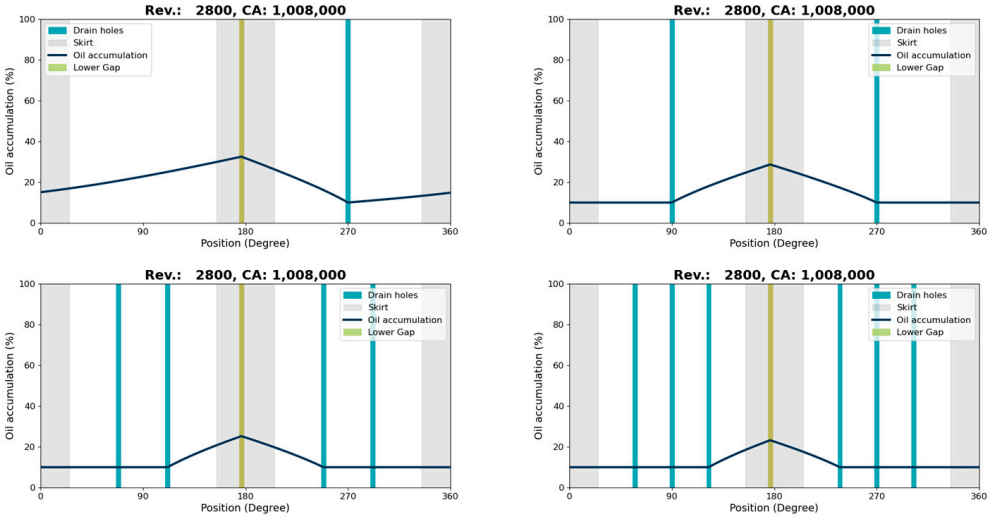

Figure 30. Piston with different number of drain holes: 1 (**top-left**), 2 (**top-right**), 4 (**bottom-left**), and 6 drain holes (**bottom-right**) drain holes.

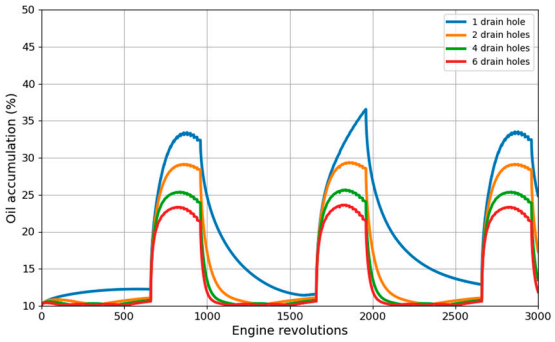

Figure 31. Effect of drain hole number on oil accumulation.

5.4. Comparison of Different Four-Drain-Hole Arrangements

This section compares two distinct four-drain-hole arrangements, as shown in Figure 32. The first design, which is the most common, places the drain holes near the skirt edge, while the second design distributes them uniformly along the pin side. The results, presented in Figure 33, show that oil accumulation is lower when the drain holes are located near the skirt edge. This is based on the assumption that oil accumulation in the groove remains constant. Additionally, since the primary oil source comes from the skirt region, placing the drain holes near the skirt edge restricts oil flow to that area. In contrast, when the drain holes are uniformly distributed along the pin side, the oil spreads over a wider area, allowing more space for accumulation.

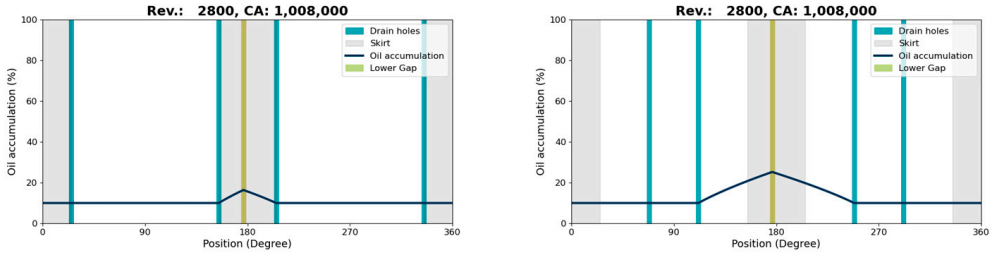

Figure 32. Two different drain holes' arrangement: Near the skirt edge (**left**), uniformly distributed along the pin side (**right**).

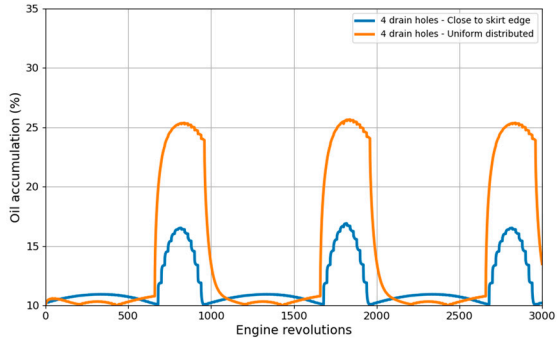

Figure 33. Effect of drain hole arrangement on oil accumulation.

5.5. Comparison of Different Viscosity

To evaluate the effect of oil viscosity, three different viscosities were compared: 0.0008 $\frac{\text{kg}}{\text{m}\cdot\text{s}}$, 0.0036 $\frac{\text{kg}}{\text{m}\cdot\text{s}}$, and 0.016 $\frac{\text{kg}}{\text{m}\cdot\text{s}}$. The results, shown in Figure 34, demonstrate that oil accumulation increases with higher viscosity and decreases with lower viscosity. Higher viscosity oils spread more slowly along the groove, leading to greater accumulation.

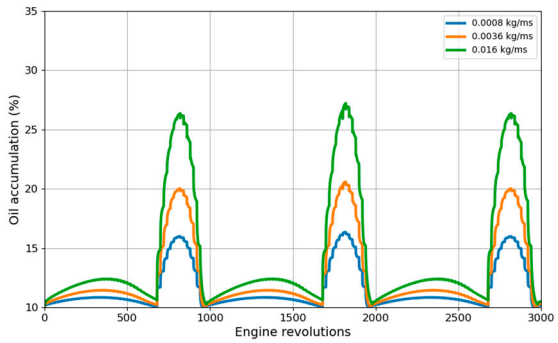

Figure 34. Effect of viscosity on oil accumulation.

5.6. Comparison of Different Rotation Speeds

In this section, various ring rotation speeds were tested to evaluate their effect on oil accumulation. The ring rotation speed is defined as the number of engine revolutions required for the oil control ring to complete one full rotation. Five different rotation speeds were considered, ranging from 2500 revolutions/rotations to 30,000 revolutions/rotations. Since the simulation involved 3000 engine revolutions, the case of 30,000 revolutions/rotation represents a stationary ring. As shown in Figure 35, the oil accumulation remains at a constant level in this scenario, where the inflow and outflow are balanced. In contrast, when the ring rotation speed is set to 2500 revolutions/rotation, two and a half peaks were observed. This is because, in this case, the lower gap starts from the position at 180 degrees, and as the ring completes one rotation, the lower gap enters the skirt region twice, resulting in higher oil accumulation.

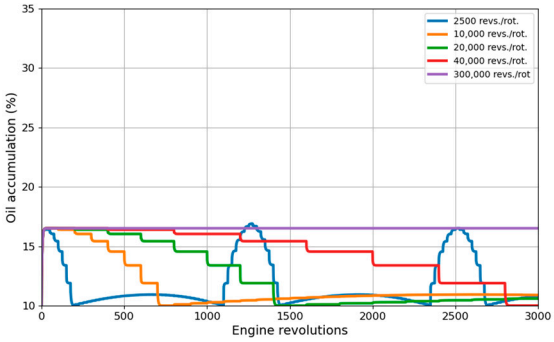

Figure 35. Effect of ring rotation speed on oil accumulation.

5.7. Comparison of Different Amounts of Oil in the Drain Holes

The drain holes are assumed to contain a constant amount of oil, as previously observed from the experimental results. Simulations were conducted with varying amounts of oil in the drain holes to understand how this affects oil accumulation in the groove. Since the drain hole is the only exit in this model, if a specific amount of oil is applied, that condition sets the minimum oil accumulation level in the groove, as shown in Figure 36. It was also observed that when a larger amount of oil (80%) is present in the groove, the peak accumulation is smaller, indicating faster oil spreading, leading to a more uniform oil layer. In contrast, when the oil amount in the drain hole is lower (5%), the peak accumulation is higher, suggesting slower oil spreading and an increased likelihood of forming oil concentration in the groove. However, these observations assume that the amount of oil in the drain holes remains constant. Further simulations are necessary to accurately model oil transport through the drain holes and develop a more realistic representation of the drain hole.

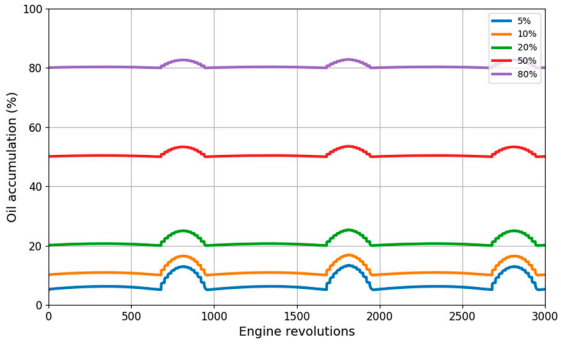

Figure 36. The effect of the amount of oil in the drain holes on oil accumulation.

6. Conclusions

This work introduced a novel one-dimensional oil distribution model for predicting oil accumulation in the TPOCR groove. The model effectively simulates oil distribution over several thousand engine revolutions, providing insights into oil behavior in the groove that would be computationally prohibitive to achieve with CFD simulations. By segmenting the TPOCR into units and leveraging CFD-derived correlations, the model captures inertia-driven oil transport along the groove.

The key findings from this research include the following:

1. Model Efficiency: The model computes oil distribution for 10,000 engine revolutions within seconds. This rapid computation allows for the quick evaluation of oil distribution under varying conditions and facilitates an iterative design process.
2. Accurate Prediction: Comparisons with CFD simulations demonstrate the model's ability to replicate observed oil distribution in the oil control ring groove with an assumption of a fixed oil volume at the drain holes.
3. Experimental Validation: The model was partially validated against experiments conducted under low load conditions at 2000 RPM. It was shown that with a proper oil exit boundary condition at the drain holes, the calculated oil accumulation patterns can match the observation accurately. As such, our future work will engage further fluid analysis and CFD to derive the boundary condition based on physics.
4. Parametric Study: The effects of oil film thickness, engine speed, and the arrangement of drain holes on oil accumulation were examined. A thicker oil film leads to higher oil accumulation. At higher engine speeds, less oil accumulates in the groove. Additionally, oil accumulation decreases as the number of drain holes increases. The arrangement of drain holes also influences oil accumulation, with placement closer to the skirt helping to reduce oil accumulation in the groove. Oil viscosity also has a significant impact, with higher viscosity leading to increased oil accumulation.

In conclusion, the one-dimensional oil distribution model developed in this study provides a tool for analyzing and predicting oil distribution in the TPOCR groove. The model's efficiency and accuracy in simulating long-term oil distribution offer essential insights for optimizing TPOCR designs and enhancing engine lubrication strategies. Future improvements should focus on incorporating more realistic boundary conditions for drain holes and gaps. Additionally, integrating the effects of gas flow into the model could further enhance its applicability to real-world scenarios. Lastly, while the oil distribution model predicts oil distribution along the groove, the TPOCR models, such as the ones developed by Zhang and Tian [14,15], capture ring dynamics and oil transport within contact regions. Combining these models is expected to provide a more comprehensive understanding of oil transport mechanisms.

Author Contributions: T.-Y.Y. conducted the CFD simulations and developed numerical models; M.L. designed and prepared the experiments. T.-Y.Y. and M.L. wrote the manuscript; T.T. supervised and revised the manuscript. All authors have read and agreed to the published version of the manuscript.

Funding: This research was supported by Mercedes-Benz and the Consortium on Lubrication in Internal Combustion Engines at the Sloan Automotive Laboratory, Massachusetts Institute of Technology. The consortium members were Mahle, Shell, Rolls-Royce Solutions, Toyota, Volkswagen Group, Volvo Trucks, and Weichai Power.

Data Availability Statement: The original contributions presented in the study are included in the article, further inquiries can be directed to the corresponding author.

Acknowledgments: This work was supported by Mercedes-Benz and the Consortium on Lubrication in Internal Combustion Engines in the Sloan Automotive Laboratory, Massachusetts Institute of Technology. The consortium members were Mahle, Shell, Rolls-Royce Solutions, Toyota, Volkswagen Group, Volvo Trucks, and Weichai Power. The author sincerely thanks all the consortium members for their support and collaboration.

Conflicts of Interest: The authors declare no conflicts of interest.

Nomenclature

2D-LIF	2D Laser Induced Fluorescence
BDC	Bottom Dead Center
CAE	Computer Aided Engineering
CFD	Computational Fluid Dynamics
FEA	Finite Element Analysis
FPGA	Field-Programmable Gate Array
LOC	Lubricating Oil Consumption
TDC	Top Dead Center
TPOCR	Three-piece oil control ring
d_{flank}	Depth of flank
E	Engine speed
h	Oil film thickness
i	Unit number
L_{stroke}	Stroke length
n	Current time step
O	Oil outflow rate
μ	Oil viscosity
ρ	Oil viscosity
V	Oil volume
w_{gap}	Lower gap width

References

1. Ito, A.; Kikuhara, K.; Nishijima, S.; Hasegawa, H.; Akamatsu, H. A Study on the Mechanism of Pressure Generating Under the Oil Control Ring of a Piston in an Internal Combustion Engine. In Proceedings of the ICEF2016, ASME 2016 Internal Combustion Engine Division Fall Technical Conference, Greenville, SC, USA, 9–12 October 2016. [CrossRef]
2. Kikuhara, K.; Nishijima, S.; Hasegawa, H.; Suzuki, H.; Ito, A.; Sekiya, H.; Akamatsu, H. A Study on Lubricating Oil Behavior under the Oil Control Ring by Oil Film Pressure Measurement. *Trans. Soc. Automot. Eng. Jpn.* **2016**, *47*, 895–900. [CrossRef]
3. Kikuhara, K.; Sekiya, H.; Ito, A.; Hayashi, H. A Study on Numerical Analysis Model of the Oil Film under the Oil Control Ring Considering the Generation Mechanism of Oil Pressure. *Trans. Soc. Automot. Eng. Jpn.* **2017**, *48*, 225–232. [CrossRef]
4. Miura, K.; Ito, A.; Nakamura, Y.; Yamada, R.; Nishibe, K.; Usui, M.; Iijima, N. A Study on the Oil Film Thickness Between the Lower Rail of Oil Control Ring and Lower Flank of Oil Control Ring Groove of an Engine. *J. Eng. Gas Turbines Power* **2024**, *146*, 081017. [CrossRef]
5. Hasegawa, H.; Kikuhara, K.; Nishijima, S.; Suzuki, H.; Ito, A.; Sekiya, H.; Akamatsu, H. The Effect of the Position and Number of Oil Drain Hole on the Oil Pressure Generating under the Oil Ring with Relation to Oil Consumption. *Trans. Soc. Automot. Eng. Jpn.* **2017**, *48*, 59–64. [CrossRef]
6. Papadopoulos, I.; Becker, S.; Ehnis, H.; Kunzel, R.; Frommer, A. Influence of Oil Drain Holes on Oil Emission of a Turbocharged Gasoline Engine. *SAE Int. J. Engines* **2017**, *10*, 1948–1953. [CrossRef]
7. Miura, K.; Ohashi, T.; Hasegawa, H.; Ito, A.; Nishibe, K. A Study on the Function of Oil Drain Holes in the Oil Ring Groove of a Piston and Their Effect on Oil Consumption. In Proceedings of the 2019 JSAE/SAE Powertrains, Fuels and Lubricants, Kyoto, Japan, 26–29 August 2019; SAE International: Warrendale, PA, USA, 2019. [CrossRef]
8. Schäffer, J.; Kirner, C.; Härtl, M.; Wachtmeister, G. Development of a Measuring System for the Visualization of the Oil Film between the Piston and Cylinder Liner of a Gasoline Engine. *SAE Int. J. Engines* **2019**, *13*, 175–190. [CrossRef]
9. Li, M.; Tian, T. Effect of Blowby on the Leakage of the Three-Piece Oil Control Ring and Subsequent Oil Transport in Upper Ring-Pack Regions in Internal Combustion Engines. *Lubricants* **2022**, *10*, 250. [CrossRef]
10. Yilmaz, E.; Thirouard, B.; Tian, T.; Wong, V.W.; Heywood, J.B.; Lee, N. Analysis of Oil Consumption Behavior during Ramp Transients in a Production Spark Ignition Engine. In Proceedings of the Spring Fuels & Lubricants Meeting & Exhibition, Orlando, FL, USA, 7–9 May 2001; SAE International: Warrendale, PA, USA, 2001. [CrossRef]
11. Uhlig, B.P.; Kirner, C.; Preuss, A.; Wachtmeister, G. *Real-Time Measurement of the Piston Ring Gap Positions and Their Effect on Exhaust Engine Oil Emission*; Automotive Technical Papers; SAE International: Warrendale, PA, USA, 2018. [CrossRef]
12. Gamble, R.J.; Priest, M.; Taylor, C.M. Detailed Analysis of Oil Transport in the Piston Assembly of a Gasoline Engine. *Tribol. Lett.* **2003**, *14*, 147–156. [CrossRef]
13. Mahesh, P.V.; Fanghui, S. CFD Analysis of Oil/Gas Flow in Piston Ring-Pack. In Proceedings of the SAE 2011 World Congress & Exhibition, Detroit, MI, USA, 12–14 April 2011; SAE International: Warrendale, PA, USA, 2011. [CrossRef]
14. Tian, T.; Wong, V.W.; Heywood, J.B. Modeling the Dynamics and Lubrication of Three Piece Oil Control Rings in Internal Combustion Engines. In Proceedings of the International Fall Fuels and Lubricants Meeting and Exposition, San Francisco, CA, USA, 19–22 October 1998; SAE International: Warrendale, PA, USA, 1998. [CrossRef]

15. Zhang, W. Modeling Internal Combustion Engine Three-Piece Oil Control Ring Coupling Reduced Order Oil Transport based on Neural Network. Master's Thesis, Massachusetts Institute of Technology, Cambridge, MA, USA, 2020.
16. Fang, T. Fluid Mechanics of Lubricant Transport in Non-Contact Regions in the Piston Ring Pack Internal Combustion Engines. Ph.D. Thesis, Massachusetts Institute of Technology, Cambridge, MA, USA, 2019.
17. Mochizuki, K.; Sasaki, R.; Iijima, N.; Usui, M. Prediction and Experimental Verification for Oil Transport Volume around Three-Piece Type Oil Control Ring Affecting Lubricating Oil Consumption. *SAE Int. J. Adv. Curr. Pract. Mobil.* **2022**, *5*, 595–609. [CrossRef]
18. Zanghi, E. Analysis of oil flow mechanisms in internal combustion engines via high-speed laser induced fluorescence (lif) spectroscopy. Master's Thesis, Massachusetts Institute of Technology, Cambridge, MA, USA, 2014.
19. Hirt, C.W.; Nichols, B.D. Volume of fluid (VOF) method for the dynamics of free boundaries. *J. Comput. Phys.* **1981**, *39*, 201–225. [CrossRef]
20. Piston and Ring Standards Committee. *Internal Combustion Engines-Piston Ring-Grooves*; SAE International: Warrendale, PA, USA, 2024. [CrossRef]